Conf-740205--8

RECENT OBSERVATIONS OF PHASE TRANSFORMATIONS IN A U-Nb-Zr ALLOY*

R. A. Vandermeer
Metals and Ceramics Division
Oak Ridge National Laboratory
Oak Ridge, Tennessee 37830 USA

ABSTRACT

Dilatometry, x-ray diffraction, hardness and optical microscopy were used to characterize a polycrystalline uranium alloy containing nominally 7.5 wt % Nb and 2.5 wt % Zr. Upon quenching this alloy from the body-centered cubic (bcc) phase at 800°C, a metastable modification corresponding to a slight tetragonal distortion of the bcc lattice along with a short-range atom displacement ordering was revealed by x-ray diffraction. Minor compositional variations, differing quenching rates and low temperature aging cause important alterations in this metastable structural state. Slight depletion of the alloying elements increases the degree of tetragonality. Aging the quenched alloy initiates transformations to other anisotropic structural states. Altogether four transformation stages have been detected by dilatometry. At temperatures as low as 150°C, two stages—one beginning after a few minutes and the other after a few hours, produce a volume expansion of the alloy and a dramatic increase in hardness. The first stage has been attributed to solute clustering. The second stage corresponds to an isothermal martensitic shear transformation, resulting in a second phase which may be described

*Research sponsored by the U. S. Atomic Energy Commission under contract with the Union Carbide Corporation.

as a monoclinic modification of the α-uranium orthorhombic structure. Cellular or discontinuous precipitation is observed at temperatures between 500 and 620°C. Light rolling deformation of the quenched alloy causes an immediate crystal reorientation to take place in certain grains. Metallographic and x-ray evidence hints that this reorientation is accomplished by mechanical twinning at low strains.

INTRODUCTION

At temperatures above 775°C and below its melting point, the crystal lattice of pure uranium is bcc—the γ-phase. Upon cooling to room temperature even at the most rapid rates,[1] this phase transforms to phases of lower symmetry and hence higher degrees of anisotropy— a characteristic that is at best very undesirable for certain nuclear applications.[2]

Alloying uranium with niobium, zirconium, titanium, etc., tends to stabilize the γ-phase to lower temperatures. But excessive quantities of solute would be needed to produce a stable γ-phase at room temperature in this class of alloys. In some cases intermetallic compound formation also interferes. On the other hand, numerous attempts have been made to "quench-in" the γ-phase by rapid cooling of alloys containing lesser amounts of solute. Experience has shown that a variety of metastable products or transition phases may result.[3,4] In addition, aging these metastable structures can alter both the structure and properties of the alloy as it attempts to approach thermodynamic equilibrium. Goldberg and Massalski[3] and Rechtien and Nelson[4] have recently reviewed the status of our knowledge concerning the transformation of the γ-phase in uranium and its alloys.

Of utmost importance to the precision manufacturing requirements of parts made from uranium alloys are, among other factors, reliable property reproducibility and dimensional stability. Volume changes are generally associated with phase transformations and these can generate internal stresses and dimensional changes. It is absolutely essential therefore to describe and understand the mechanisms of phase transformations in uranium and its alloys and to discover the significant factors affecting these transitions. This fundamental knowledge will be useful for better control, less property deterioration and increased reliability of manufactured parts.

Phase transformations in uranium and its alloys are as yet not very well understood.[3] Therefore, the purpose of this work was to investigate the nature and characteristics of the phase transformations in one "commercially" important polycrystalline uranium alloy. The alloy contained nominally 7.5 wt % niobium and 2.5 wt % zirconium. We have considered in some detail the effects of metallurgical variables such as minor compositional gradients, quench rate, mechanical deformation and low temperature aging on the decomposition of the γ-phase and the metastable structural states associated with it. The main investigative tools for this research were x-ray diffraction and dilatometry. Transformation mechanisms will be proposed and where possible classified and compared with prototypes which occur in more familiar or so-called "classical" alloy systems.

The constitution of the uranium-rich portion of the U-Nb-Zr system has been investigated by Dwight and Mueller.[5] Some physical and mechanical properties of the U-7.5 wt % Nb-2.5 wt % Zr alloy were reported by Peterson and Vandervoort[6] and Peterson and Elkington.[7] C. W. Dean,[8]

utilizing primarily metallographic examination and microhardness measurements along with some x-ray diffraction analyses, determined the time-temperature-transformation behavior of the γ-phase decomposition for this alloy. A comprehensive x-ray diffraction study by Yakel[9] on quenched and aged single crystals established the crystal structures of two metastable transition phase products of γ-phase decomposition. Jackson and Boland,[10] extending the work of Peterson and others[6,7] have measured the mechanical properties of water-quenched specimens as a function of aging time and temperature, attempting to relate strengths to transformation kinetics, microstructure, and crystal structure. The low strain tensile behavior of the U–7.5 wt % Nb–2.5 wt % Zr alloy after γ-quenching was examined by Albright and Stein[11] and Oakes.[12] Recently Girand-Herand and Guillaumin[13] used electron microscopy to characterize the products of γ-phase transformation in this alloy.

EXPERIMENTAL PROCEDURE

MATERIALS

All specimens used in this study were obtained from the Development Division of the Oak Ridge Y-12 Plant. The uranium alloy containing nominally 7.5 wt % U and 2.5 wt % Zr was prepared by skull-casting a vacuum arc-melted charge.[14] The cast ingot was subsequently homogenized at 1000°C and then hot rolled at 800°C. The resulting slab did exhibit a macroscopic but gradual surface-to-center chemical composition variation of the solute elements. However, the severe micro-banded inhomogeneity observed by Dean[8] was not present. The machined specimens for this study were selected from approximately the same locations in the slab relative to its thickness.

Analyses for trace impurities and interstitial solute levels were not carried out on these specific alloy specimens. They would be expected, however, to be approximately the same as those reported by Dean[8] for a similar alloy.

HEAT TREATMENT AND MISCELLANEOUS

The specimens for x-ray diffraction examination, deformation studies, optical microscopy and microhardness tests were wafers approximately 2.5 x 2.5 x 0.37 cm. The grains were equiaxed and the grain size as measured by lineal analysis generally fell between 30 and 60 μ. These samples were initially subjected to an elevated temperature heat treatment to stabilize the γ-phase. This heat treatment was carried out in a horizontal tube furnace maintained at 800°C for times of at least 1 hr. Oxidation of the wafers was minimized by passing argon through the furnace tube at an approximate flow rate of 50 liters/hr. Next, the wafers were quenched into either (1) a 10% brine (or caustic) solution, (2) an equilibrated ice water mixture, (3) hot water maintained at 94°C, or (4) still air at 24°C. In a few cases, specimens were first quenched into a sodium nitrite-potassium nitrate salt bath at an intermediate temperature in the range 400 to 550°C, held there for 30 min and then quenched into the ice water mixture.

All heat treated and quenched specimens were electropolished to remove the inevitable oxide film that developed during these handling procedures. The electrolyte was composed of 45% (by volume) orthophosphoric acid, 40% sulfuric acid and the remainder water. Usually 30 to 40 μ were removed from each surface by the electropolish.

Low temperature aging of the γ-treated and quenched uranium-niobium-zirconium alloy was carried out at 154°C in a boiling bromobenzene

refluxing bath, at 188°C in boiling decahydronapthalene and at 350°C in the salt bath. The temperature variation in the boiling organic liquid baths was ± 0.1°C and in the salt bath ± 5°C. No contamination aside from slight oxidation of the alloy by the aging baths was detected. After each aging treatment the samples were again electropolished. In the interest of economy and to minimize sample-to-sample variations due to the minor compositional gradients in the alloy, a single wafer was used at each temperature. Thus each quenched sample was aged for a number of successive time periods. Accumulated aging times reached as long as 37 days.

Microhardness measurements were obtained on the quenched and the quenched and aged samples using a Gries microhardness tester and a 1000-g load. Sixteen individual measurements were made for each sample tested and both the mean value and the 99% confidence limits on the mean are reported.

Metallographic samples of selected heat treated conditions were prepared by conventional methods. These were usually electropolished and electroetched in a 10% oxalic acid in water solution just prior to examination.

Deformation was accomplished by rolling a water-quenched specimen on a hand-operated, 2-high rolling mill. X-ray and microhardness data were obtained from the rolling plane surfaces of this specimen after permanent reductions in thickness of 1 and 3%. After each rolling reduction approximately 25 μ were removed from each surface by electropolishing.

X-RAY DIFFRACTION

The primary thrust of the x-ray diffraction work was to determine the lattice parameters of the quenched and the quenched and aged alloys. All intensity measurements were made at room temperature on a conventional

Norelco diffractometer. Nickel-filtered, copper x-radiation was used at 35 kV and 20 mA. Each sample was scanned at a rate of 1/8° per min over the 2θ range 15 to 130°. The diffracted beam intensity was detected with a gas-type proportional counter after having been screened by a pyrolytic graphite monochromator which greatly reduced background scatter. The diffracted beam signal was amplified, passed through a single-channel-analyzer discriminating circuit and collected by a digital ratemeter. After summing the signal for 6 sec and averaging, the information was both printed out and punched onto paper tape by a teletypewriter and the ratemeter automatically reset to zero. Thus each data point represented the diffracted intensity in counts per second averaged over 0.0125° 2θ. In each run, the ratemeter and the diffractometer were synchronized so data could be taken automatically. Finally, the collected data was processed with the IBM 360 computer and plotted by a Calcomp plotter.

Apparent lattice parameters were calculated for all diffraction peaks of reasonable intensity and were obtained from measurements of the angular location of the peak maxima on these plots. To correct for sample displacement from the diffractometer axis and other systematic errors, these lattice parameters were plotted against the function, cot θ cos θ, and linearly extrapolated to cot θ cos θ = 0 to obtain a truer value for the lattice parameter.[15] In the cases of non-cubic crystal structures, the method of extrapolation described by Taylor[16] was utilized with some modification. A correction for the slight misalignment of the diffractometer was also applied to the data. It was obtained by comparing the diffraction data from a well annealed silicon standard with established handbook values.

The breadth of certain diffraction peaks was estimated by measuring the width of the peak at one half of maximum intensity.

DILATOMETRY

Specimens for the dilatometric phase of this study were hollow cylinders 1-cm long with an outside diameter of 0.4 cm and a wall thickness of 0.1 cm. The dilatometer was a commercial instrument purchased from Labtronics, a Division of Theta Industries, Inc. Individual samples were longitudinally spring-loaded onto a silica push-rod assembly which was frictionlessly mounted to a linear-variable-differential-transformer (LVDT). The expansion (or contraction) of the sample was transferred through the push rod to the core of the LVDT where it was converted into an electrical signal. Next the signal was amplified and demodulated and finally it was continuously displayed on a strip chart recorder. A micrometer mounted to the LVDT assembly permitted calibration of the length measurement.

The sample was heated by a high frequency induction coil in a bell jar vacuum system at pressures always less than 5×10^{-5} torr. A Pt–Pt 10% Rh thermocouple which had been spot welded to the outside wall of the sample, not only measured the sample temperature but also controlled the temperature through a stepless, SCR power supply. The thermocouple output was displayed on the same strip chart recorder that the length change was. The recorder had a maximum speed of 2.5 cm/sec but could be slowed by changing gears.

Rapid cooling was achieved by the flow of helium quenching gas through the hollow silica push rod assembly onto the interior surface of the hollow specimen. Cooling rates could be varied by controlling the gas flow rate. The maximum cooling rate attainable with this equipment upon quenching from 800°C was 400°C/sec.

Both quenching and quenching plus aging experiments were carried out inside the dilatometer. Prior to being quenched, the as-machined alloy cylinders were brought to 800°C or above and held for 10,000 sec to promote a recrystallized grain structure. Aging was generally accomplished after quenching to room temperature at the maximum rate of cooling. Reheating to the aging temperature usually required times of less than 4 sec. The length, temperature, and time were all measured by hand from the strip chart output.

RESULTS

Quenching Studies

The x-ray diffraction pattern, i.e., intensity versus 2θ, from a polycrystalline sample of this alloy quenched from the γ-phase at 800°C into ice water is depicted in Fig. 1. This pattern is characteristic of the so-called γ_d^o* phase described by Yakel[9] in terms of the tetragonal unit cell shown in the inset of Fig. 1. In addition to the strong peaks, F, weak, broad reflections designated S are also apparent in this pattern. These result, according to Yakel,[9] because the atoms in the side faces of the unit cell are not centered but are slightly displaced from the center in the c-axis direction. Note, the atoms in the front and rear faces are displaced upwards (plus z-direction), while those in the left and right sides are displaced downward (minus z-direction). The atoms in the top and bottom faces remain centered and undisplaced.

Tangri[18] has proposed a different structure for γ_d^o in alloys of uranium containing molybdenum. His interpretation was based on a chemical specie ordering of atoms of different scattering power. The lack of

---

*The nomenclature here used is adopted from Lehman and Hills.[17]

intensity at 2θ positions marked O in Fig. 1 definitely rules out Tangri's structure for γ_d^o in this alloy. Were Tangri's model applicable, weak peaks at least as strong as those designated S should appear at O positions. Instead, we conclude that Yakel's correlated atom displacement model for γ_d^o more aptly accounts for the polycrystalline x-ray pattern.

Figure 2 illustrates the plotting method used to obtain the lattice parameters, a and c/a, from the experimental data of Fig. 1. Of particular note is the negative deviation of many of the S peaks from the line describing the F peak behavior. The extrapolated values of a and c/a, neglecting the S peaks, were 4.937 Å and 0.6296, respectively. The 99% confidence limit on a is ± 0.002 Å. The atomic volume per atom as calculated from these data was 20.83 $Å^3$/atom.

The microstructure of this uranium-niobium-zirconium alloy quenched into ice water after γ-treatment at 800°C is shown in Fig. 3. No metallographic evidence of phase transformation such as a banded or acicular microstructure was apparent after quenching. The precipitates noted in the photomicrograph were identified by x-ray analysis as Zr(Nb,U)C and UO_2. Zr(Nb,U)C has a cubic NaCl structure with a lattice parameter of 4.637 Å. Microhardness measurements yielded a DPH number of 181 ± 4 for this quenched alloy.

Because of the macroscopic composition gradients which existed in the initial ingot, through-the-thickness composition differences were unavoidable for the wafer-shaped samples examined in this work. Thus the two broad faces of the wafer specimen were effectively "different" alloys. The niobium and zirconium levels of these two faces, side A and side B, were determined nondestructively by means of x-ray fluorescence analysis. The analysis was achieved by comparing the fluorescent intensities from

the wafer surfaces with those from a well homogenized standard whose composition had been determined by the usual chemical means. Side A contained approximately 7.3 wt % Nb and 2.6 wt % Zr--a composition close to the nominal values for this alloy. Side B by comparison was depleted in the sclute elements by a total of 0.4 wt %. It analyzed 6.9 wt % Nb and 2.6 wt % Zr. The x-ray and other results discussed above and in Figs. 1-3 were obtained from side B.

The characteristics of this material were found to be profoundly influenced by the amount of solute. Even the above mentioned relatively minor differences caused significant variation in the nature of the quenched structure. Furthermore, changing the quenching medium, thereby affecting the cooling rate, resulted in observable modifications in structure for specimens of essentially the same composition. These effects are summarized in Fig. 4 and Table 1. Certain features of these results are worth underscoring:

1. The microhardness of side A was always 30 to 50 points higher than side B.

2. The solute depleted material (side B) tended to a higher degree of tetragonality (its c/a ratios were lower) than the solute richer material (side A). Also with respect to this parameter, quenching rate, as reflected by the various quenching media, appeared to have less of an effect on side A than on side B. (It should be pointed out that when the c/a ratio is 0.7071, the lattice may be regarded as bcc instead of tetragonal; the c parameter equals one half the face diagonal of the top or bottom face in the unit cell of Fig. 1.)

3. The (012) S x-ray peaks were not as broad for the solute-depleted material as they were with the solute-richer regions of the alloy. Line

broadening measurements on (121) S peaks indicated they usually had 20 to 30% less breadth than did the (012) peaks.

4. The most dramatic difference between sides A and B was produced with ice water quenching.

5. Caustic (or brine) quenching tended to minimize the structural differences between the two sides yet there was a 49-point difference in DPH values.

6. With the exception of ice water quenching, the atomic volume was approximately the same for both sides.

7. Because of the relatively low quenching rate, effects due to low temperature aging reactions were reflected in samples cooled in still air.

8. The breadth of the x-ray peaks labeled F were remarkably narrow after hot water quenching of side A material.

An interesting structure approaching closely that of the elevated temperature γ-phase was developed in the side A alloy upon quenching into hot water. The x-ray pattern is illustrated in Fig. 5 and the plot to obtain the lattice parameter is shown in Fig. 6. This pattern differed from that of the γ-phase because of the additional weak, broad diffraction maxima (peaks labeled S) that were evident. These peaks required a doubling of the three γ-unit cell edges to describe the structure which has been named γ^{O} (sometimes referred to as γ^{S}). Yakel[9] has demonstrated that the observed diffracted intensity from single crystals of this phase could be explained by small, correlated displacements of certain atoms from specific sites along $\langle 100 \rangle$ directions. As with the γ_d^{O} phase, Tangri[18] has also proposed a chemical specie ordering model for γ^{O}. Again, this model seems inappropriate for the same reasons acknowledged earlier in this paper for γ_d^{O}—a finding which agrees with Yakel's earlier conclusions.

The x-ray diffraction patterns obtained for quenching conditions which produced c/a ratios approaching 0.7071 posed certain difficulties in their analysis. For one thing, the close-by pairs of peaks generally expected from slightly tetragonal lattices were not resolvable. Instead the x-ray pattern appeared upon cursory examination to describe a bcc lattice. But detailed scrutiny of the diffraction peaks revealed them to be asymmetric. The angular direction of the asymmetries, i.e., the shift to higher or lower angles, fell into a definite pattern which could be explained by a tetragonal distortion of the bcc structure. As example, data from side B quenched into caustic solution, i.e., fastest quenching rate, are plotted in Fig. 7. The upper plot based on the γ^o structure clearly does not describe the data as well as the lower one based on the tetragonal lattice γ_d^o. The tetragonal indices assigned to each of the asymmetric peaks were chosen on the basis of which line of the close-by tetragonal pair was the strongest. The possibility that the scatter of data in the upper plot might have arisen instead from residual stresses due to the drastic quench was considered. That idea was discarded when it was realized that for a bcc lattice the (022), (224), (044), and (246) peaks, i.e., the solid points in the upper plot of Fig. 7, should all lie on the same straight line if only residual stresses were present.[15] Thus, the tetragonal description and the lattice parameters calculated therefrom were accepted.

When the quenching of specimens of the uranium-niobium-zirconium alloy was interrupted by an intermediate salt bath heat treatment for 30 min before the final ice water quench to room temperature, the resultant γ_d^o structure possessed a higher degree of tetragonality. As Fig. 8 shows, the c/a ratio was smaller, the lower was the salt bath

temperature. The 30 min hold at these intermediate temperatures, i.e., 400 to 550°C was short enough to prevent significant transformation of the γ-phase to other structural states (see Fig. 11). The x-ray diffraction pattern for a sample quenched to an intermediate temperature of 415°C before the final ice water quench to room temperature appears in Fig. 9. When contrasted to Fig. 1, it was noted that some significant changes in intensity had occurred with certain of the diffraction lines. Particularly apparent was the intensity decrease of the (020), (220), (131), and (240) peaks.

Dilatometric studies of the uranium-niobium-zirconium alloy during quenching from 800°C are summarized in Fig. 10. Here $\Delta\ell/\ell_o$ is plotted versus temperature for four different quenching rates. The parameter t_q is the time required for the specimen to cool to 400°C. To place these quenching studies into perspective with those on the wafer-shaped samples already described, it should be realized that the hot water quench would correspond approximately to something intermediate to the two left-hand curves. Cooling in still air should roughly match the $t_q = 170$ curve. Bear in mind that quenching into ice water or caustic solutions gave more rapid quenching rates than could be achieved in the dilatometer.

Several points are worth noting about this dilatometric data: (1) For rapid cooling the length varied continuously with temperature (the two left-hand curves). (2) At the slower cooling rates (the two right-hand curves) there is dimensional change evidence, i.e., an inflection point, for the onset of a phase transformation. The arrows denote the temperature for the start of such transformations. (3) On reheating, the slowest cooled specimen exhibited an unusual hysteresis in length versus temperature behavior; whereas the $t_q = 170$ test showed very nearly

reversible, i.e., almost no hysteresis, characteristics. (4) The apparent thermal expansion coefficient for the γ-phase, i.e., the slope of the curves in Fig. 10 at the highest temperatures, varied with cooling rate and was larger the slower the cooling rate.

Aging Studies

Upon aging the uranium-niobium-zirconium alloy in the dilatometer after quenching from 800°C, dimensional changes ensued which could be attributed to phase transformations. Four separate stages were distinguished in the temperature range 160 to 600°C. A TTT diagram is depicted in Fig. 11. The points in this diagram correspond to the times when approximately 5% of the transformation has happened. At temperatures below 385°C the transformations (stages I and II) caused an expansion of the sample. Above this temperature contraction was observed during aging (stages III and IV). Representative length change versus aging time data is plotted in Fig. 12 for five different temperatures. A discussion of the nature of these transformations is deferred to later in this paper.

Supplimentary information regarding the low temperature transformations was obtained from x-ray diffraction studies of the solute-depleted (side B) regions of the alloy. Figure 13 shows the variation of the lattice parameters and atomic volume for the as-quenched γ_d^o "phase" as a function of aging time at 154 and 188°C. Of particular note during stage I, should be the $\underline{a}$ parameter increase, the $\underline{c}/\underline{a}$ decrease, and the overall atomic volume increase. In stage I no evidence for the formation of a distinct second phase was indicated by the x-ray work.

The response of the $\underline{a}$ lattice parameter to aging in stage II was more complex; $\underline{c}/\underline{a}$ continued to decrease and the atomic volume of the γ_d^o phase was now smaller than in the quenched condition. Coincident with the onset

of stage II was the appearance of diffraction effects which may be interpreted as due to the formation of a new phase. The 2θ positions where new diffraction peaks emerged were consistent with positions expected from an α-uranium-like (probably the monoclinic α″) phase. An x-ray pattern obtained from a specimen aged 120 hr at 350°C was indexed in terms of a monoclinic structure and yielded the following lattice constants: $\underline{a}$ = 2.863 Å, $\underline{b}$ = 5.900 Å, $\underline{c}$ = 4.966 Å, and γ (the non-orthogonal angle) = 90.8°. Considerable line broadening and shifts in x-ray peak positions of the γ_d^o phase also became gradually apparent during stage II aging. These were presumably due to the transformation strains imposed when α″ forms from γ^o. Dilatometry estimated that the volume change associated with this phase transition may be as high as 0.75%. Further information about the stage II phase change was provided by the emergence of a microstructure such as that shown in Fig. 14. Finally, in both stage I and stage II substantial hardening was observed (see Fig. 15).

Deformation Studies

Some effects of mechanical working on the structural parameters of the γ_d^o "phase" are displayed in Figs. 16 and 17 while additional data are tabulated in Table 2. Earlier it was pointed out that the S-lines and F-lines did not describe the same straight line in the plot of $\underline{a}$ versus cos θ cot θ. Of interest here it should be noted that rolling deformation caused the S and F peaks to merge within the limits of our experimental accuracy. Obscuring this effect somewhat is the fact that rolling introduced scatter into the data, i.e., the 95% confidence limit in $\underline{a}$ was not so narrow. Also, a slight curvature of the specimen was apparent after rolling and this was manifested in the data by an increase in the slope of the $\underline{a}$ versus cos θ cot θ plots.

Another important observation had to do with the dramatic decrease of intensity noted for certain x-ray reflections as a result of this small amount of rolling reduction. Figure 17 illustrates this effect for the (220) reflection. It was estimated that the (220) peak decreased in intensity by about a factor of 8 after only a 3% rolling reduction while the (002) intensity changed not at all. Those x-ray peaks that underwent drastic decreases always had ℓ indices that were zero, i.e., (220), (240), etc., or very much less than h + k, e.g., (131). Like the (002), the intensity of the (113) with its strong ℓ component remained approximately the same.

DISCUSSION

Quenching Studies

The present results support the view of Yakel[9] concerning the description of γ^o and γ_d^o structures and their generation from the parent γ phase. Conceptually these transition phases are produced when linear displacement waves, i.e., small atom position shifts carried out cooperatively, traveling in $\langle 001 \rangle_\gamma$ directions become "frozen in" and correlated with respect to displacements in next-nearest neighbor rows and alternate rows beyond these. The γ^o structure results when the displacements nucleate with equal probability in each of the three $\langle 001 \rangle_\gamma$ directions, i.e., there are three variants possible. If within each γ-grain (or subgrain) on the other hand the atom movements are correlated along only one particular $[001]_\gamma$ direction, i.e., only one variant is operative, the bcc lattice collapses to produce a tetragonal lattice, i.e., the γ_d^o structure. The existence of displacement ordering in metallurgical systems has only recently been recognized. The ω-phase formation from a

precursor bcc lattice in certain titanium and zirconium alloys is one example.[19,20] That reaction can be described as an ordered sequence of ⟨111⟩ displacements.

In their review of ordering reactions in unfamiliar systems Richman and Davies[21] were led to regard γ^o as the displacement analog of short-range chemical specie order and γ_d^o as the long-range analog. We will adopt and develop this analogy in the further interpretation of our data.

As with chemical order one of the immediate consequences of the displacement ordering transition is the introduction of anti-phase domain boundaries into the material. Two types may be distinguished; inter-variant and intra-variant. The first type must by definition be present in the γ^o structure. Several subtypes of the intra-variant domain walls can also exist and these are depicted schematically in Fig. 18. The figure also demonstrates an alternate way of visualizing the displaced structure (γ_d^o in this case). This description is in terms of the stacking of corrugated and smooth (002) atomic planes. If displacement order were complete, only alternate layers would be corrugated and the corrugations would be periodic over the entire plane (I). The presence of intra-variant anti-phase domains alters this stacking sequence (II and II) or introduces a "phase shift" in the corrugations on the rumpled plane (IV). The presence of anti-phase domain boundary may cause the spacing changes responsible for the separation of the S peaks from the F peaks in Fig. 2. In the chemical ordering of B2 structures a theoretical analysis indicated that anti-phase domain boundary could produce unusual x-ray peak shifts which affect superlattice reflections differently than the fundamental peaks.[22,23]

In chemically ordered alloy systems and specifically where a disordered high-temperature cubic phase becomes tetragonal upon long-range ordering at low temperatures, a relationship was found[24,25] between the degree of long-range order and the ratio of lattice parameters c and a. In addition the degree of long-range chemical order in the "classical system" Cu_3Au depends on the anti-phase domain size,[26] i.e., amount of domain boundary area. If these two principles can be applied to displacement order in the U–7.5 wt % Nb–2.5 wt % Zr alloy, then a plot of c/a versus β (012)S should exhibit a correlation. Evidence that this is so is illustrated in Fig. 19. This correlation presupposes that the excessive breadth or diffuseness of the (012)S diffraction peak is primarily due to domain size effect. The physical interpretation of the correlation suggested by Fig. 19 is that for those conditions producing lesser amounts of inter-variant domain boundary the degree of tetragonality is increased (c/a decreases) and a higher degree of long-range displacement order exists. The question still remaining is: When is displacement ordering complete, or in other words, what is the minimum c/a ratio for this alloy?

Quenching a solid body requires a thermal gradient so that heat will flow out. Thermal stresses can be generated in such a body during sudden cooling. As the quench takes place, the cool outside contracts more than the warm inside so the surface is placed in tension and the center in compression. If the warm interior can undergo plastic flow at this point, then later, when the interior shrinks as it cools, it puts a compressive residual stress on the already cold peripheral layers. Should these compressive stresses be sufficiently high, additional plastic deformation would take place in the surface layers. If, on the other hand, the

thermal stresses never exceed the flow stress of the material, the behavior will always be elastic, and no residual stresses would arise. Those specimens that were quenched in two steps—first into a salt bath at some intermediate temperature and then into ice water showed anomalous intensity reductions for certain x-ray peaks compared to those quenched directly into ice water (compare Fig. 9 with Fig. 1). It is suggested that a complex stress state imposed during quenching caused plastic deformation of the surface layers for the specimen whose quench was interrupted. This suggestion may be inferred when it is recognized that the intensity reduction patterns observed upon rolling deformation corresponded exactly to those in specimens quenched in two stages.

The specimens quenched directly into ice water, while they may have been subjected to residual stress, were affected to a much lesser extent as no apparent permanent deformation of the surface layers was evident. It may also be important in this respect that the former had a higher degree of long-range displacement order, i.e., lower c/a ratio, and hence greater anisotropy than the latter. This high order may be a result of the 30-min hold at the intermediate temperature.

It is apparent from Fig. 4 that quench rate and minor solute fluctuations are important variables in the displacement ordering phenomena. An explanation of the role that quenching rate exerts on the displacement ordering process must, however, await further work of both a theoretical and experimental nature. It does seem that factors such as vacancy supersaturation, solute diffusion, the nature of the nucleation mechanism and quenching stresses must somehow be involved.

Aging Studies

We turn now to a discussion of the phase transformations that occur on aging the quenched U–7.5 wt % Nb–2.5 wt % Zr alloy. In contrast to the work of Dean[8] and Girand-Herand and Guillaumin,[13] our results based on a dimensional instability criterion suggested four stages of transformation rather than three. It is frequently informative to examine the kinetics of transformations in terms of the Avrami equation[27]

$$X_v = 1 - \exp - Bt^n \qquad (1)$$

where X_v is the volume fraction of transformation, t is the aging time, and B and n are constants. The kinetics of transformations can be well-studied by dilatometry if the atomic volume of the parent phase is sufficiently different from the average atomic volume of the product phases. Then at a constant temperature we can write

$$X_v = \frac{V - V_o}{V_f - V_o} \qquad (2)$$

where X_v is the volume fraction tranformed at any instant, V is the instantaneous volume of the specimen, V_o is the volume of the parent phase and V_f is the volume of the fully transformed product. Since length changes are small, it can be shown that Eq. (2) may be simplified to

$$X_v = \frac{\ell - \ell_o}{\ell_f - \ell_o} \qquad (3)$$

where the ℓ's are the specimen lengths corresponding to the above mentioned V's.

The dilatometric data on the kinetics of transformation in each of the four aging stages have been evaluated according to the Avrami equation. The resulting log-log plots are shown in Fig. 20 for aging temperatures of 579, 435, 347, 271, 190, and 160°C. Table 3 lists the values of n in

Eq. (1) as determined from these and other experimental plots. It is immediately obvious that at 271°C more than one transformation stage was operative. Only at the two highest and two lowest temperatures did the data obey Avrami-type kinetics over a substantial portion of the transformation.

The transformation in stage IV, i.e., 500°C < T < 620°C has many of the same characteristics as a discontinuous precipitation reaction (sometimes called cellular precipitation). Microstructurally, colonies of a lamellar structure nucleate at grain boundaries and inclusion interfaces and grow as hemispheres into the center of the grains.[8,13] The alternate plates in these colonies are presumably a solute-poor orthorhombic phase and a solute-rich bcc phase.[8] This transformation also has characteristics similar to the eutectoid decomposition of austenite to form pearlite in steel. Cellular precipitation of tin from a lead-tin solid solution has been widely studied.[28] The kinetic transformation law deduced from electrical resistivity measurements in that system gave an Avrami constant n equal to three. The present results on stage IV kinetics of the U-Nb-Zr alloy yielded the same Avrami exponent. All these findings imply that the rate-controlling step in stage IV was thermally activated and interface controlled, i.e., the slowest atomic process in this cellular growth was the transfer of atoms along and/or across the interface between the parent phase (γ) and the duplex cells containing the product phases ($\gamma + \alpha$). Furthermore, the microstructural evidence[8,13] in conjunction with n = 3 strongly suggested that nucleation of the cells was site-saturated, i.e., all nucleation sites became active upon the start of the transformation and no further nucleation was possible.

Interpretation of the aging transformation in stage III, i.e., $385 < T < 510°C$ was speculative. The scale of the transformation product was difficult to resolve by optical metallography[8,13] but electron microscopy indicated it to be composed of disks of a supersaturated α-phase aligned in bands and having a definite crystallographic orientation relationship with the matrix phase.[13] The observed kinetic law with $n = 2$ was not inconsistent with this microstructure if during precipitation the disks became larger without becoming appreciably thicker, i.e., two-dimensional edge-wise growth, and nucleation was site-saturated.

The transformation occurring in stage II showed interesting differences in kinetic behavior. During the early stages, the rate of transformation was very high (the apparent Avrami constant n is high) but in the latter stages the transformation slowed dramatically, and the apparent n became small (< 1). The initially high value for n, i.e., $n > 4$ implied that the nucleation process was the over-riding kinetic factor controlling the start of this transformation.[27] The high Avrami constant, the dramatic retardation of rate and the banded, twin-like microstructures accompanying this transformation (Fig. 14) led to the conclusion that this was an isothermal (martensitic) shear transformation. The transformation product was the monoclinic α'' phase. Its formation from γ during the quenching of other uranium alloys is well known.[3] In those studies it was proposed to be shear-like and diffusionless. Its relegation to isothermal transformation status in this alloy rather than being a quenched-in phase as in alloys containing less solute[29] must be tied to the difficulty of nucleating the new phase. The apparently "stiffer" lattice of a higher solute-containing alloy such as this one evidently made shear more difficult, hence stifling α'' formation in the quenching of that alloy.[3]

Once nucleated, the transformation product formed during stage II aging could continue the transformation at higher temperatures ($T > 385°C$)—temperatures where it could not have nucleated in the first place but where instead stage III would have interceded. It is because of this unusual behavior that there was extreme hysteresis between the cooling and heating dilatometric test data for T_q = 425 sec. in Fig. 10. This behavior could also resolve some of Howlett's[30] unexplained dilatometric observations in U-Mo alloys.

An effort was made to determine the activation energy associated with the transformation to α''. Figure 21 plots the reciprocal of the time to start the transformation versus the reciprocal of the absolute temperature. The activation energy determined from the slope of this curve was 8100 cal/mole. This activation energy was considerably lower than that of the bulk interdiffusion coefficient measured in U-Nb alloys.[31] This finding supported the view that α'' nucleated by a shear that required no long-range diffusion. There was some suggestion in the latter periods of stage II, i.e., where the slope of the curve for 347°C in Fig. 20 drops below 1, that long-range solute diffusion may be involved.

Isothermal shear (martensitic) transformations have been studied in iron-nickel-manganese alloys. Recent theoretical work on such transformations by Pati and Cohen[32] showed that isothermal C-curve behavior as opposed to athermal transformation on cooling with its distinct M_s temperature, depended on the potency of pre-existing embryos, i.e., size of the largest embryo and/or the driving force. Less potent embryos or low driving force favored isothermal behavior. The explanation in terms of the concept of lattice "stiffness" or resistance to shear in uranium alloys suggested above seems to fit in with these views if embryo size is inversely related to lattice "stiffness."

Previous studies[8,13] only recognized one transformation stage during aging at temperatures below about 400°C. Our experimental data clearly indicated two such stages. An explanation for stage I was sought in terms of solute clustering even though an alternate proposal considering the transformation to be a short-range to long-range displacement order transition, i.e., $\gamma_o \rightarrow \gamma_d^o$ might appear more attractive. This alternate proposal was rejected for the following reasons: (1) Upon ordering with its simultaneous removal of anti-phase domain boundary a contraction of the alloy would be expected; instead an expansion was apparent (Fig. 12) in spite of the fact that c/a decreased (Fig. 13). (2) Detailed analysis of the kinetics of stage I did not agree with that expected from ordering theory.

The solute-clustering mechanism for stage I had considerable merit in our opinion because: (1) The U-Nb-Zr alloy system is monotectoid in nature. Therefore if chemical terms alone are considered, spontaneous separation into solute-rich and solute-poor regions at low temperatures is thermodynamically anticipated; even spinodal decomposition may be possible. (2) Solute-clustering has been observed by Ammons in U-Ti alloys.[33] (3) The Avrami constant n = 2/3 was in substantial agreement with clustering kinetics reported for Al-Ag alloys.[34] (4) Turnbull[35] derived a theoretical kinetic law for clustering, assuming that the process corresponded to the growth of larger clusters at the expense of smaller ones. The driving force for the process would be related to the interfacial energy between cluster and matrix. The derived equation can be written in terms of the volume fraction transformed as

$$X_v = 1 - \frac{1}{(1 + kt)^{1/3}} \qquad (4)$$

where t is the time and k is related to the atomic mobility of solute. Figure 22 plots the stage I dilatometry data for aging at 160°C according

to this equation. Even though deviations were observed at long times, the initial stages seemed to be in excellent agreement with Turnbull's theory. Data at 190 and 218°C were also in substantial agreement. (5) The observed activation energy for stage I determined from the temperature dependence of k was 14,000 cal/mole. The ratio of this value to that for bulk solute interdiffusion (estimated from results in U-Nb alloys[31]) is about the same ratio (~ 0.4) observed in other clustering systems.[28]

Thus from both a kinetic point of view and a thermodynamic one, clustering of solute appears to be a reasonable explanation for the stage I behavior. The reduction of $\underline{c}/\underline{a}$ on aging then would be due to solute depletion rather than additional long-range displacement order. But no detailed microstructural information was available from this work. Thus, questions still remain concerning the morphology, size and composition of the clusters. Other questions are: Does the solute segregate preferentially to anti-phase domain walls? Do Nb and Zr segregate together or separately?

Deformation Studies

One of the effects of deformation by rolling on the γ_d^o structure indicated that crystals of certain orientations are very unstable to the stress state imposed during rolling. Immediate reorientation occurred in these grains for only 1% plastic deformation. Examination of the microstructure after this extent of rolling revealed the presence of numerous twin-like markings which were not there before rolling. Some grains contained a profusion of these markings while others had few or none. We believe these to be deformation twins and not transformation twins or α'' plates for the following reasons. The markings were very

thick compared to α'' plates and had a different habit plane. No x-ray evidence for a new phase was detected even though the volume fraction of plates was sufficiently high to be detectable if they were indeed a new phase. Finally, the microhardness was smaller after the first 1% deformation by rolling; whereas α'' when formed on aging caused a large increase in hardness.

Mechanical twinning is a common mode of plastic deformation especially in anisotropic materials. The present x-ray results could be explained, qualitatively at least, if mechanical twinning occurred on (101) planes in a $[10\bar{1}]$ direction. This twinning mode has been observed for other tetragonal structures.[36] If the stress state in rolling may be regarded ideally as a compression stress in the normal direction and a tensile stress in the rolling direction, then grains with [110] directions parallel to the normal direction would readily twin, undergoing immediate reorientation in the process. Grains with [001] directions parallel to the normal direction would not be in a position to twin, because the twinning shear could not produce the imposed shape change. Essentially then [110] grains would be unstable during rolling while [001] would be stable, and this is in agreement with our observations (Fig. 17).

SUMMARY

1. The decomposition of the γ-phase in a uranium alloy containing 7.5 wt % Nb and 2.5 wt % Zr was studied by x-ray diffraction and dilatometry.

2. The effects of minor compositional variations and different quenching rates on the degree of displacement order after quenching the alloy from 800°C were described.

3. Low temperature aging studies analyzed from a kinetic viewpoint allowed some understanding to be gained concerning the mechanisms of the aging transformations.

4. Some results were presented indicating that crystal reorientation by mechanical twinning was an operative deformation mechanism during the earliest stages of rolling.

ACKNOWLEDGMENT

The partial support of this work by W. J. Hulsey and A. M. Ammons of the Development Division of the Y-12 Plant is gratefully acknowledged. Thanks is due to J. C. Ogle, A. Wood and W. Farmer who aided in some of the experimental phases of this work. Appreciation is expressed to C. J. McHargue, J. V. Cathcart, H. L. Yakel, and R. W. Carpenter for critically reviewing the manuscript.

REFERENCES

1. Duwez, Pol, "The Effect of the Rate of Cooling on the Allotropic Transformation Temperatures of Uranium," J. APPL. PHYS., 24, no. 2 (1953), 152-156.

2. REACTOR HANDBOOK, 2nd ed., Vol. 1, Materials, ed. by C. R. Tipton, Jr. New York: Interscience Publishers (1960), 87-211.

3. Goldberg, Alfred, and Massalski, Tadeusz B., "Phase Transformations in the Actinides," Lawrence Radiation Laboratory, University of California, Livermore. Report UCRL-72557, June 29, 1970.

4. Rechtien, J. J., and Nelson, R. D., "Phase Transformations in Uranium, Plutonium, and Neptunium," MET. TRANS., 4 (1973), 2755-2765.

5. Dwight, A. E., and Mueller, M. H., "Constitution of the Uranium-Rich U-Nb and U-Nb-Zr Systems," Argonne National Laboratory, Lemont, Illinois, U. S. Atomic Energy Commission. Report ANL-5581, October 1957.

6. Peterson, C.A.W., and Vandervoort, R. R., "The Properties of a Metastable Gamma-Phase Uranium Base Alloy: U-7.5 Nb-2.5 Zr," University of California, Lawrence Radiation Laboratory, Livermore. Report UCRL-7869, May 1964.

7. Peterson, C.A.W., and Elkington, W. E., "Physical and Mechanical Properties of U-7.5 wt % Nb-2.5 wt % Zr Alloy," University of California, Lawrence Radiation Laboratory, Livermore. Report UCRL-14724, February 1966.

8. Dean, C. W., "A Study of the Time-Temperature-Transformation Behavior of a Uranium-7.5 weight percent Niobium-2.5 weight percent Zirconium Alloy," Union Carbide Corporation Nuclear Division, Oak Ridge Y-12 Plant, U. S. Atomic Energy Commission. Report Y-1694, October 1969.

9. Yakel, Harry L., "Crystal Structures of Transition Phases Formed in U/16.60 at. % Nb/5.64 at. % Zr Alloys," J. NUCL. MAT., 33 (1969), 286-95.

10. Jackson, Ross J., and Boland, Joseph F., "Transformation Kinetics and Mechanical Properties of the Uranium-7.5 Niobium-2.5 Zirconium Ternary Alloy," Dow Chemical, Rocky Flats Division, Golden, Colorado. Report RFP-1652, December 1971.

11. Albright, C., and Stein, C., "The Low Strain Tensile Behavior of U-7.5 wt pct Nb-2.5 wt pct Zr.," MET. TRANS., 3 (1972), 2217-2223.

12. Oakes, Jr., R. E., "The Anomalous Mechanical Properties of U-7.5 wt % Nb-2.5 wt % Zr Alloy," Union Carbide Corporation Nuclear Division, Oak Ridge Y-12 Plant, U. S. Atomic Energy Commission. Report Y-1732, September 1970.

13. Giraud-Heraud, F., et Guillaumin, J., "Formation de Phases de Transition dans l'alliage U-7.5% Nb-2.5% Zr," ACTA MET., 21, no. 9 (1973), 1243-1252.

14. Cadden, J. L., "Melting of Uranium Alloy," this volume.

15. Wagner, C.N.J., "Analysis of the Broadening and Changes in Position of Peaks in an X-Ray Powder Pattern," LOCAL ATOMIC ARRANGEMENTS STUDIED BY X-RAY DIFFRACTION, ed. by J. B. Cohen and J. E. Hilliard. New York: Gordon and Breach Science Publishers, Metallurgical Society Conferences, Vol. 36 (1966) 219-268.

16. Taylor, A., X-RAY METALLOGRAPHY. New York: John Wiley and Sons, Inc. (1961), 185-88.

17. Lehmann, J., and Hills, R. F., "Proposed Nomenclature for Phases in Uranium Alloys," J. NUCL. MATER., 2, no. 3 (1960), 261-268.

18. Tangri, K., "Les Phases Gamma Metastables dans les Alliages d'Uranium Contenant du Molybdene," MEM. SCI. REV. MET., 58, no. 6 (1961), 469-78.

19. De Fontaine, D., Paton, N. E., and Williams, J. C., "The Omega Phase Transformation in Titanium Alloys as an Example of Displacement Controlled Reactions," ACTA MET., 19 (1971), 1153-1162.

20. Williams, J. C., De Fontaine, D., and Paton, N. E., "The ω-Phase as an Example of an Unusual Shear Transformation," MET. TRANS., 4, (1973), 2701-2708.

21. Richman, R. H., and Davies, R. G., "Ordering Reactions in Unfamiliar Systems," MET. TRANS., 4, (1973), 2731-2746.

22. Mohanty, G. P., and Schmidt, R. A., "Diffraction from Planar Faults in the β-Brass Type Ordered Structures," J. APPL. PHYS., 41, (1970), 3573-3581.

23. Rothman, R. L., Marion, R., and Cohen, J. B., "Broadening and Shifting of Diffraction Profiles from Anti-Phase Domain Boundaries or Stacking Faults in a B2 Structure," in PROCEEDINGS CONFERENCE ON ORDERED ALLOYS AT BOLTON LANDING, New York, (1970), 149-167.

24. Roberts, B. W., "X-Ray Measurements of Order in CuAu," ACTA MET., 2, (1954), 597-603.

25. Guttman, Lester, "Order-Disorder Phenomena in Metals," in SOLID STATE PHYSICS, Vol. 3, ed. by F. Seitz and D. Turnbull. New York: Academic Press, Inc., (1956), 145-223.

26. Davies, R. G., and Stoloff, N. S., "Order and Domain Hardening in Cu_3Au Type Superlattice Alloys," ACTA MET., 11, (1963), 1347-1353.

27. Christian, J. W., THE THEORY OF TRANSFORMATIONS IN METALS AND ALLOYS. Oxford: Pergamon Press (1965), 471-495.

28. Ibid., 606-669.

29. Jackson, Ross J., "Reversible Martensitic Transformations between Transition Phases of Uranium-Base Niobium Alloys," Dow Chemical, Rocky Flats Division, Golden, Colorado. Report RFP-1535, December 1970.

30. Howlett, B. W., "A Study of the Shear Transformations from the Gamma-Phase in Uranium-Molybdenum Alloys Containing 6.0–12.5 at % Molybdenum," J. NUCL. MATER., 35, (1970), 278-292.

31. Peterson, N. L., and Ogilvie, R. F., "Diffusion Studies in the Uranium-Niobium(Columbium) System," TRANS. TMS-AIME, 218, (1960) 439-444; "Diffusion in the Uranium-Niobium(Columbium) System," TRANS. TMS-AIME, 227, (1963) 1083-1087.

32. Pati, S. R., and Cohen, M., "Nucleation of the Isothermal Martensitic Transformation," ACTA MET., 17, (1969), 189-199; "Kinetics of Isothermal Martensitic Transformation in an Iron-Nickel-Manganese Alloy," ACTA MET., 19, (1971) 1327-1332.

33. Ammons, A. M., "Precipitation Hardening of Uranium-Titanium Alloys Containing Less Than 1.0 Weight Percent Titanium," Union Carbide Corporation, Oak Ridge Y-12 Plant, U. S. Atomic Energy Commission. Report Y-1850, September 1972.

34. Herman, Herbert, and Fine, Morris E., "An Acoustical Study of Low-Temperature Age-Hardening after Reversion in Al-6 at Pct Ag," TRANS. TMS-AIME, 218 (1960) 44-50.

35. Turnbull, David, "Phase Changes," SOLID STATE PHYSICS, Vol. 3, ed. by F. Seitz and D. Turnbull. New York: Academic Press, Inc. (1956), 225-306.

36. Kelly, A., and Groves, G. W., CRYSTALLOGRAPHY AND CRYSTAL DEFECTS. London: Longman Group Limited, (1970), 290-312.

37. Kollie, T. G., Private communication.

TABLE 1

Characteristics of Uranium–7.5 wt % Niobium–2.5 wt % Zirconium Alloy Quenched from 800°C

Quench Medium	Apparent* Quench Rate (°C/sec)		Lattice■ Parameters		Atomic■ Volume $(Å)^3$	Micro-Hardness■ (DPH)	X-Ray Line Breadth■ °2θ			Side
	600°C	200°C	a(Å)	c/a			(012)S	(121)S	(220)F	
10% Caustic (or Brine)	3730	612	4.916	0.703	20.88	177 ± 3	1.75	1.20	0.63	B
			4.910	0.705	20.87	226 ± 7	1.81	1.50	0.40	A
Ice Water	1920	459	4.935	0.6937	20.84	181 ± 4	1.35	1.07	0.40	B
			4.899	0.7057	20.73	220 ± 7	2.20	1.87	0.34	A
Hot Water 94°C	80	319	4.906	0.703	20.76	195 ± 6	1.55	1.12	0.72	B
			4.896	0.7071	20.75	235 ± 5	2.10	1.65	0.20	A
Still Air	51	3.2	4.932	0.690	20.70	192 ± 8	1.46	1.08	0.83	B
			4.910	0.700	20.70	218 ± 8	1.65	1.46	0.83	A

*Estimated from ASM Metals Handbook, 1948 edition, p. 617.

■Average of several samples.

TABLE 2

Effect of Rolling Deformation on

Uranium-7.5 wt % Niobium-2.5 wt % Zirconium

Condition	Micro-Hardness (DPH)	Apparent Lattice Parameters		Atomic Volume $(Å)^3$	Line Breadths (°2θ)		
		a (Å)	c/a		(002)f	(220)f	(012)s
As-Quenched	155 ± 4	4.9424 ± 0.0034	0.6900	20.83	0.44	0.40	0.98
As-Quenched and Rolled 1%	143 ± 3	4.9323 ± 0.0076	0.6906	20.72	0.45	0.56	1.00
As-Quenched and Rolled 3%	153 ± 4	4.9206 ± 0.0104	0.6925	20.63	0.85	NM	1.30*

*Very asymetric.

NM - Not measurable.

TABLE 3

Avrami Constant n for

Uranium–7.5 wt % Niobium–2.5 wt % Zirconium Aging Stages

Temperature (°C)	160	190	218	271	347	435	470	551	579
Measured Avrami Constant, n	0.67	0.67	0.67	NM	6.5* 0.5**	2.0	2.0	2.3	3.0
Stage	I	I	I	I&II	II	III	III	IV	IV

*Short times.

**Long times.

NM-Not measured.

Fig. 1. X-ray intensity versus 2θ for uranium–7.5 wt % niobium–2.5 wt % zirconium alloy held 1 hr at 800°C and quenched into ice water (side B).

Fig. 2. Lattice parameter extrapolation curves for U–7.5 wt % Nb–2.5 wt % Zr alloy (side B) quenched from 800°C into ice water. Filled circles--F peaks; triangles, S peaks.

Fig. 3. Microstructure of U–7.5 wt % Nb–2.5 wt % Zr alloy quenched from 800°C into ice water. Electropolished and etched in 10% oxalic acid solution. Bright field. 500X.

Fig. 4. Variation of c/a, atomic volume and (012) line breadth for side A and B as a function of quench medium for U–7.5 wt % Nb–2.5 wt % Zr quenched from 800°C.

Fig. 5. X-ray intensity versus 2θ for a U–7.5 wt % Nb–2.5 wt % Zr alloy held 1 hr at 800°C and quenched into hot water at 94°C. Side A.

Fig. 6. Lattice parameter extrapolation curve for U–7.5 wt % Nb–2.5 wt % Zr alloy (side A) quenched from 800°C into hot water at 94°C. Filled circles, F peaks; triangles, S peaks.

Fig. 7. Lattice parameter extrapolation curves for U–7.5 wt % Nb–2.5 wt % Zr alloy (side B) quenched from 800°C in a 10% brine solution. Indexed as tetragonal (bottom) and cubic (top). Circles, F peaks; triangles, S peaks.

Fig. 8. Plot of c/a versus intermediate hold temperature for U–7.5 wt % Nb–2.5 wt % Zr quenched from 800°C into a salt bath at intermediate temperature, held 40 min and then quenched into ice water.

Fig. 9. X-ray intensity versus 2θ for a U–7.5 wt % Nb–2.5 wt % Zr alloy held 1 hr at 800°C, quenched into salt at 415°C and held 30 min and then quenched into ice water. Side B.

Fig. 10. Length change versus temperature for U–7.5 wt % Nb–2.5 wt % Zr for four different cooling rates. Open symbols, cooling; closed symbols, heating for t_q = 170 and 425 only. Arrows indicate onset of transformation.

Fig. 11. Time-temperature-transformation diagram for a U–7.5 wt % Nb–2.5 wt % Zr alloy as determined by dilatometry. Filled symbols, resistivity data of Kollie.[37]

Fig. 12. Length change versus aging time at five different temperatures for a U–7.5 wt % Nb–2.5 wt % Zr alloy quenched from 800°C.

Fig. 13. Plots of x-ray lattice parameters and atomic volume versus aging time at 154 and 188°C for a U–7.5 wt % Nb–2.5 wt % Zr alloy (side B) quenched from 800°C.

Fig. 14. Microstructure of U–7.5 wt % Nb–2.5 wt % Zr alloy quenched from 800°C and aged for 502 hr at 154°C. Electropolished and etched in 10% oxalic acid solution. Bright field. 500X.

Fig. 15. Diamond pyramid hardness versus aging time for a quenched U–7.5 wt % Nb–2.5 wt % Zr alloy aged at 154 and 188°C.

Fig. 16. Effect of 1% rolling deformation on the lattice parameters of a quenched U–7.5 wt % Nb–2.5 wt % Zr. Solid points, F peaks; open triangles, S peaks.

Fig. 17. Effect of 1 and 3% rolling deformation on the x-ray intensity of the (220) and (002) planes of a quenched U–7.5 wt % Nb–2.5 wt % Zr alloy. Peak identification: (121)S, (220)F, (002)F, (002)F, and (012)S, respectively.

Fig. 18. Projection of (002) planes illustrating the subtypes of intravariant antiphase domain boundaries for displacement ordered U–7.5 wt % Nb–2.5 wt % Zr alloy. Open points correspond to the plane of paper; filled points represent the first plane above and below the plane of paper.

Fig. 19. Plot of c/a versus line breadth of the (012)s peak for U–7.5 wt % Nb–2.5 wt % Zr after quenching from 800°C. Filled circles, side A; open circles, side B.

Fig. 20. Avrami equation plots of the transformation kinetics of a quenched and aged U–7.5 wt % Nb–2.5 wt % Zr alloy at six temperatures

Fig. 21. Plot of transformation rate versus reciprocal of absolute temperature for stage II aging of a quenched U–7.5 wt % Nb–2.5 wt % Zr alloy.

Fig. 22. Plot of stage I transformation kinetics according to Turnbull's clustering theory Eq. (4) in text.

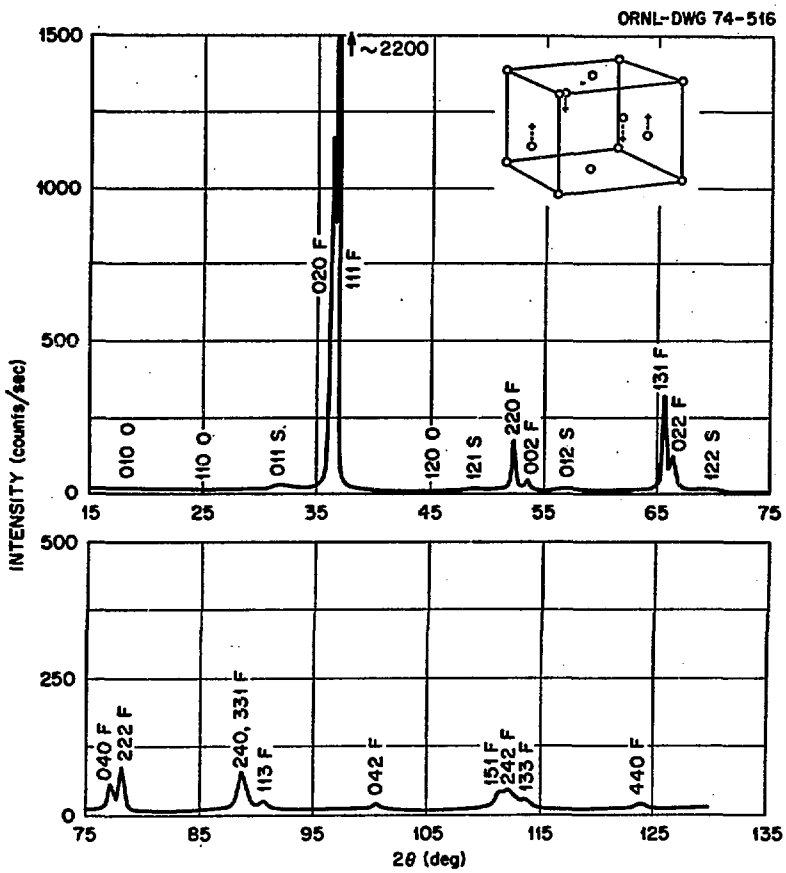
ORNL-DWG 74-516
INTENSITY (counts/sec)
1500
1000
500
0
~2200
020 F
111 F
010 O
110 O
011 S.
120 O
121 S
220 F
002 F
012 S
131 F
022 F
122 S
15
25
35
45
55
65
75
500
250
0
040 F
222 F
240, 331 F
113 F
042 F
151 F
242 F
133 F
440 F
75
85
95
105
115
125
135
2θ (deg)

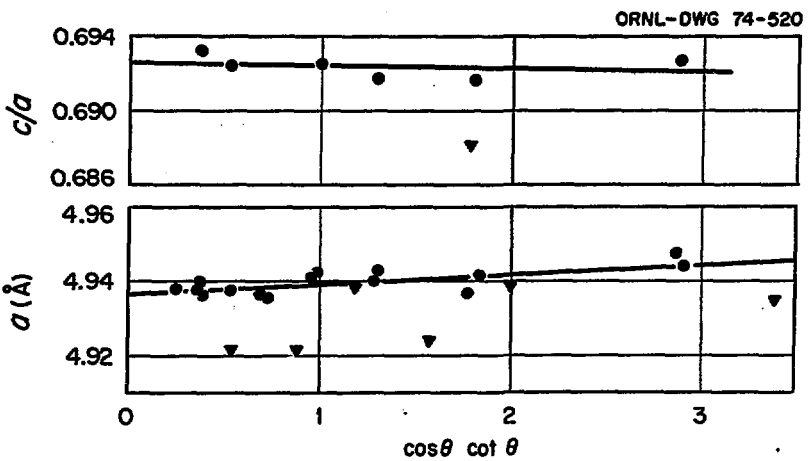
ORNL-DWG 74-520
0.694
0.690
0.686
c/a
4.96
4.94
4.92
a (Å)
0
1
2
3
cosθ cot θ

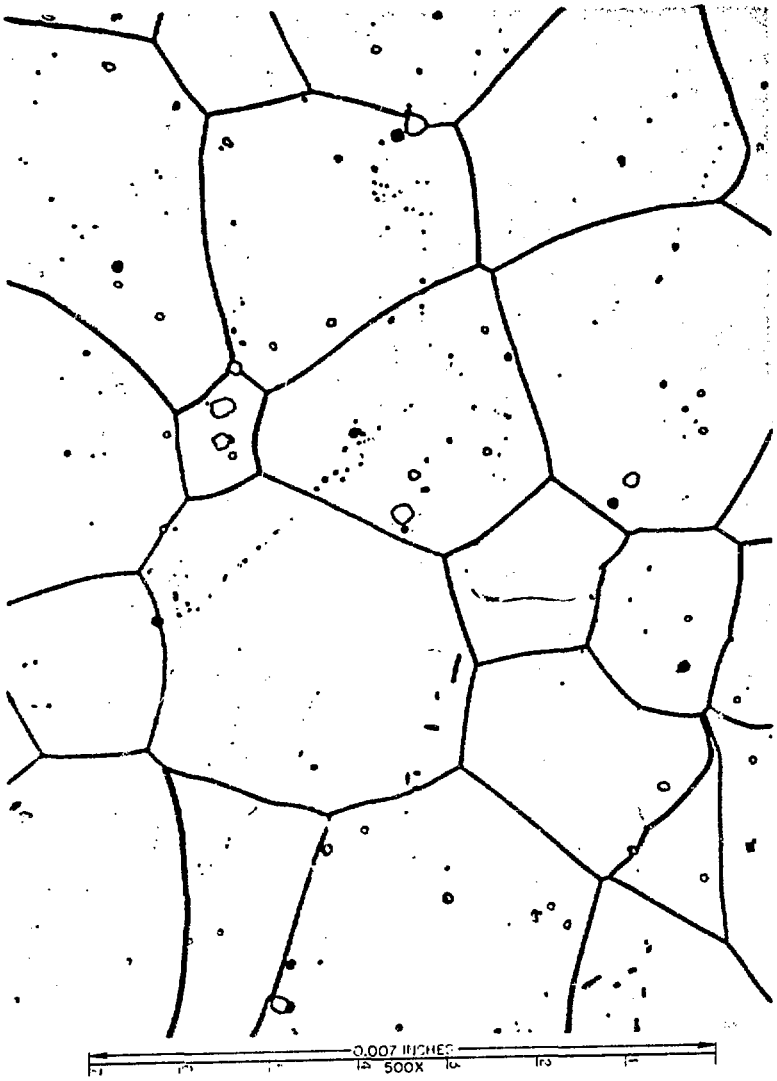
0.007 INCHES
500X

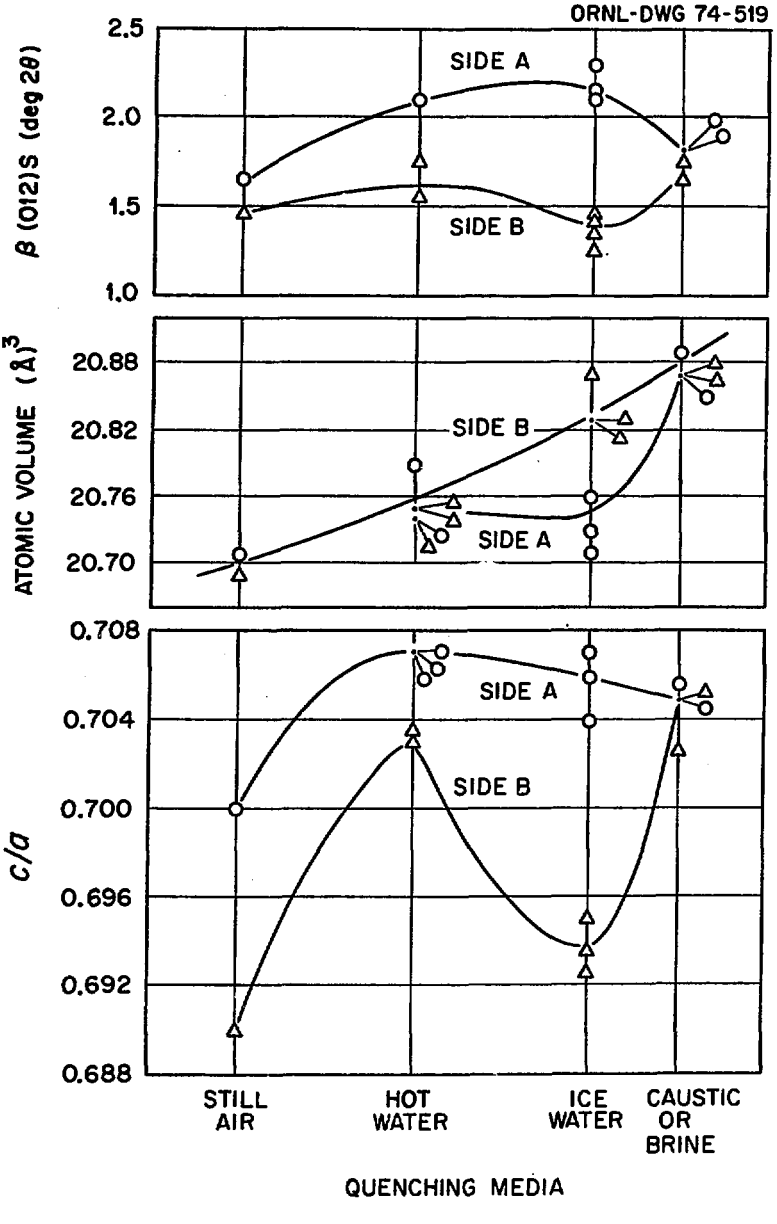
ORNL-DWG 74-519
β (012)S (deg 2θ)
2.5
2.0
1.5
1.0
SIDE A
SIDE B
ATOMIC VOLUME (Å)3
20.88
20.82
20.76
20.70
SIDE B
SIDE A
c/a
0.708
0.704
0.700
0.696
0.692
0.688
SIDE A
SIDE B
STILL AIR
HOT WATER
ICE WATER
CAUSTIC OR BRINE
QUENCHING MEDIA

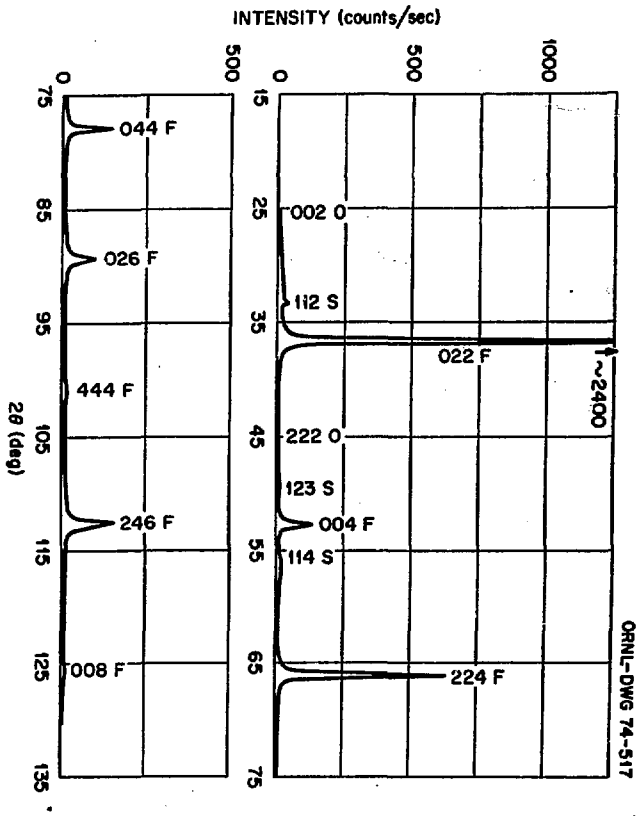
INTENSITY (counts/sec)
0
500
1000
15
25
35
45
55
65
75
002 0
112 S
022 F
~2400
222 0
123 S
004 F
114 S
224 F
0
500
75
85
95
105
115
125
135
044 F
026 F
444 F
246 F
008 F
2θ (deg)
ORNL-DWG 74-517

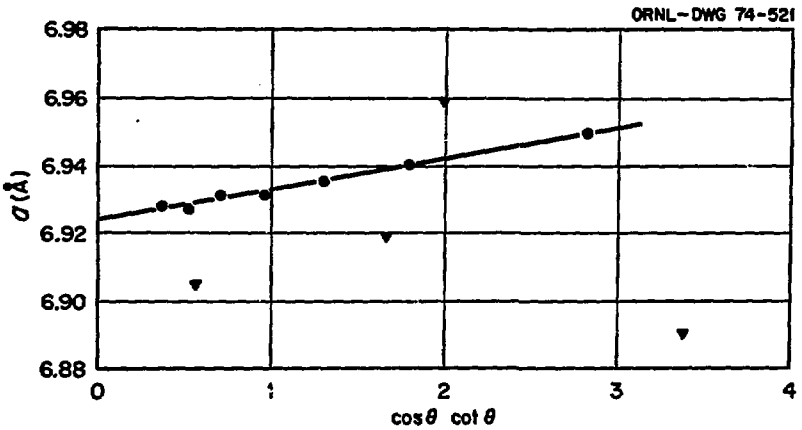
ORNL-DWG 74-521
6.98
6.96
6.94
6.92
6.90
6.88
σ(Å)
0
1
2
3
4
cosθ cotθ

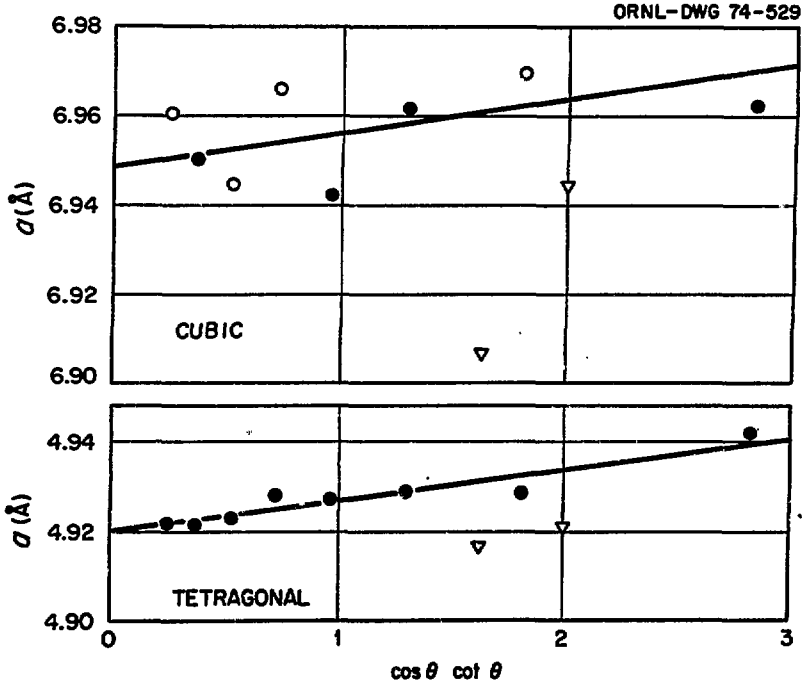
ORNL-DWG 74-529
6.98
6.96
6.94
6.92
6.90
a (Å)
CUBIC
4.94
4.92
4.90
a (Å)
TETRAGONAL
0
1
2
3
cos θ cot θ

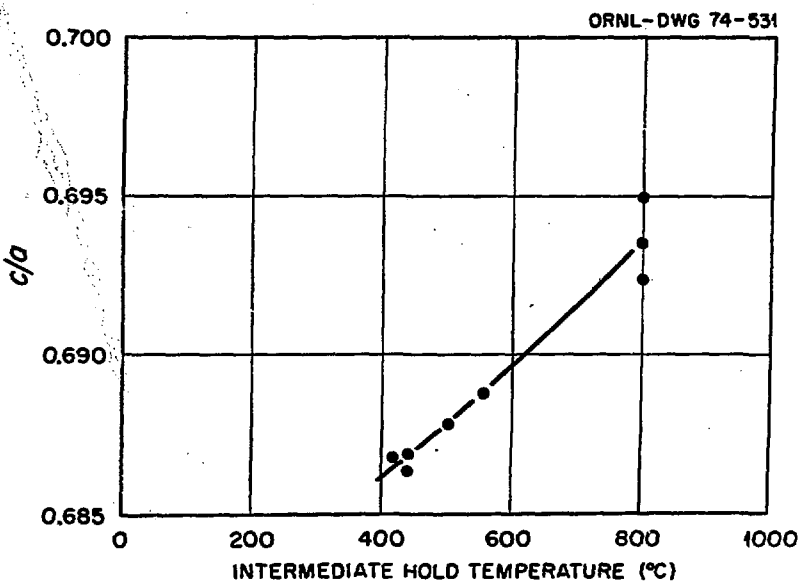
ORNL-DWG 74-531
0.700
0.695
0.690
0.685
c/a
0
200
400
600
800
1000
INTERMEDIATE HOLD TEMPERATURE (°C)

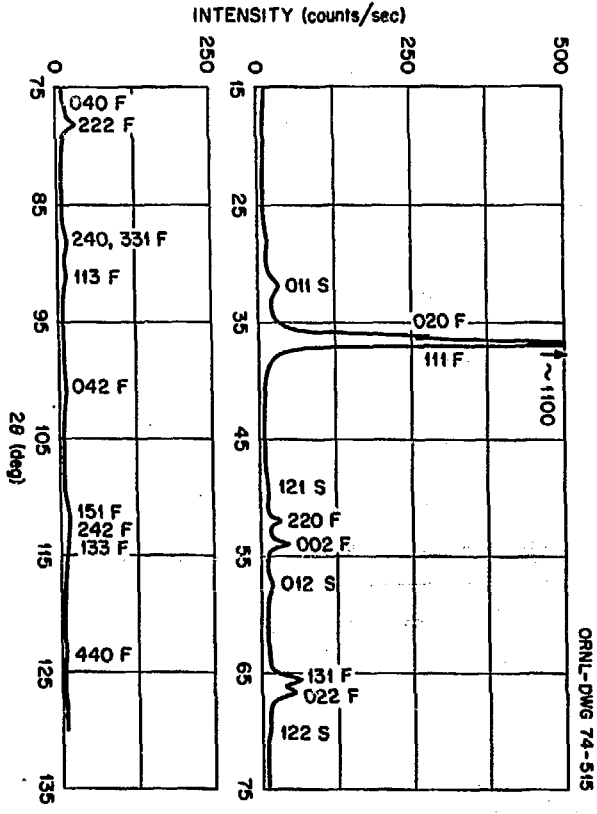
INTENSITY (counts/sec)
0
250
500
2θ (deg)
040 F
222 F
240, 331 F
113 F
042 F
151 F
242 F
133 F
440 F
011 S
020 F
111 F
~1100
121 S
220 F
002 F
012 S
131 F
022 F
122 S
ORNL-DWG 74-515

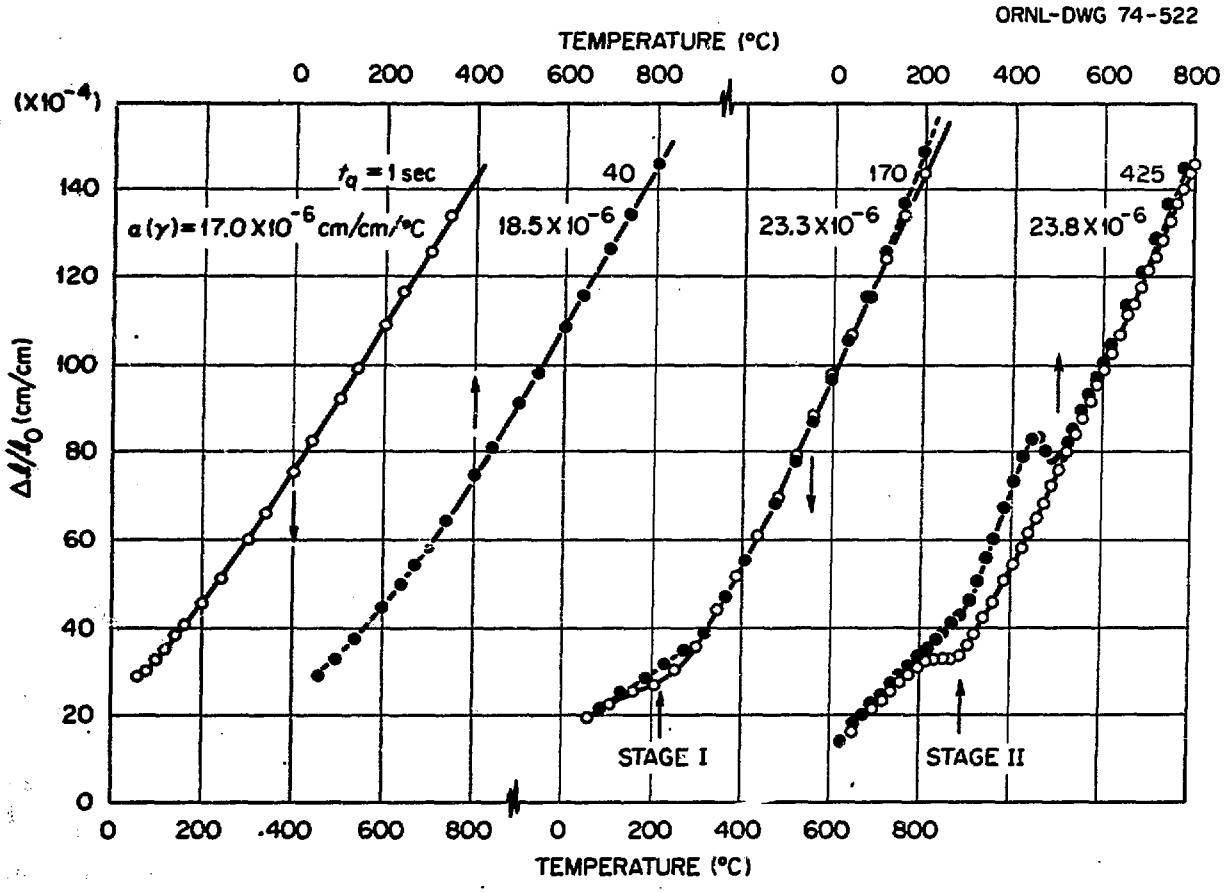
ORNL-DWG 74-522
TEMPERATURE (°C)
0 200 400 600 800
0 200 400 600 800
(X10⁻⁴)
140
120
100
80
60
40
20
0
ΔL/L₀ (cm/cm)
t_q = 1 sec
$\alpha(\gamma) = 17.0 \times 10^{-6}$ cm/cm/°C
40
18.5×10^{-6}
170
23.3×10^{-6}
425
23.8×10^{-6}
STAGE I
STAGE II
0 200 400 600 800
0 200 400 600 800
TEMPERATURE (°C)

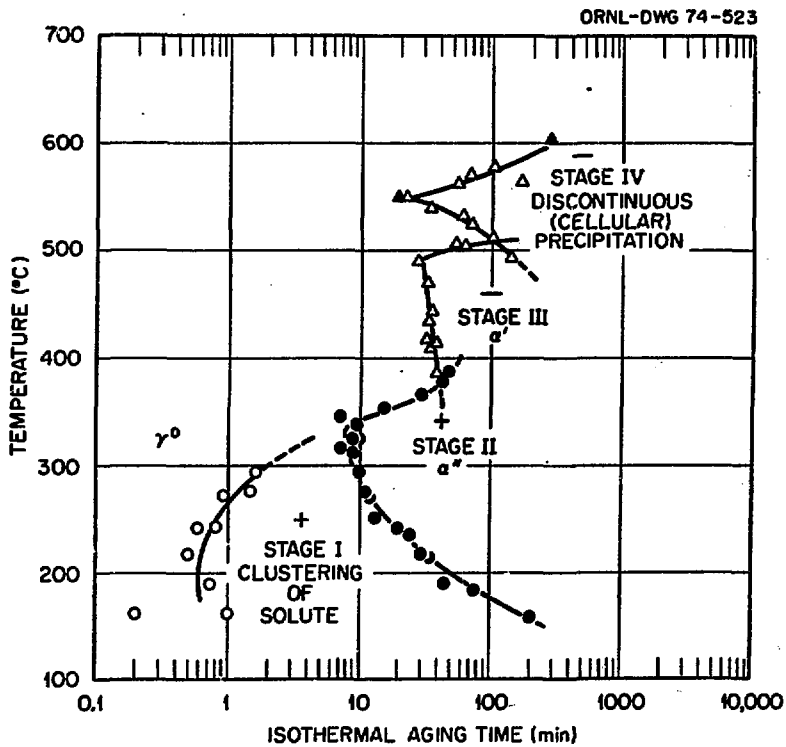
ORNL-DWG 74-523
700
600
500
400
300
200
100
TEMPERATURE (°C)
0.1
1
10
100
1000
10,000
ISOTHERMAL AGING TIME (min)
STAGE IV
DISCONTINUOUS
(CELLULAR)
PRECIPITATION
STAGE III
α'
STAGE II
α''
γ°
STAGE I
CLUSTERING
OF
SOLUTE

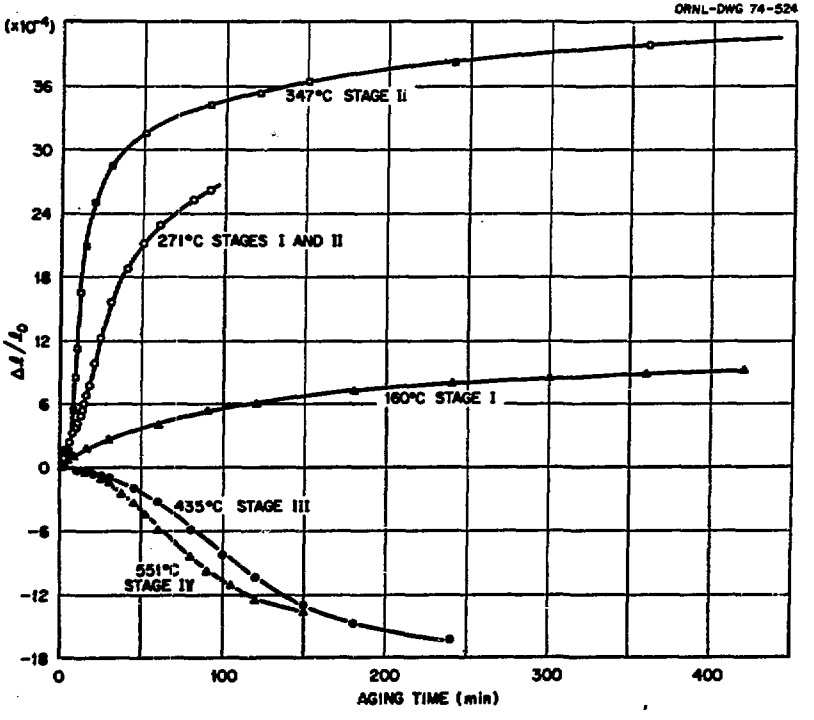
ORNL-DWG 74-524
(x10⁻⁴)
36
30
24
18
12
6
0
-6
-12
-18
Δl/l₀
347°C STAGE II
271°C STAGES I AND II
160°C STAGE I
435°C STAGE III
551°C
STAGE IV
0
100
200
300
400
AGING TIME (min)

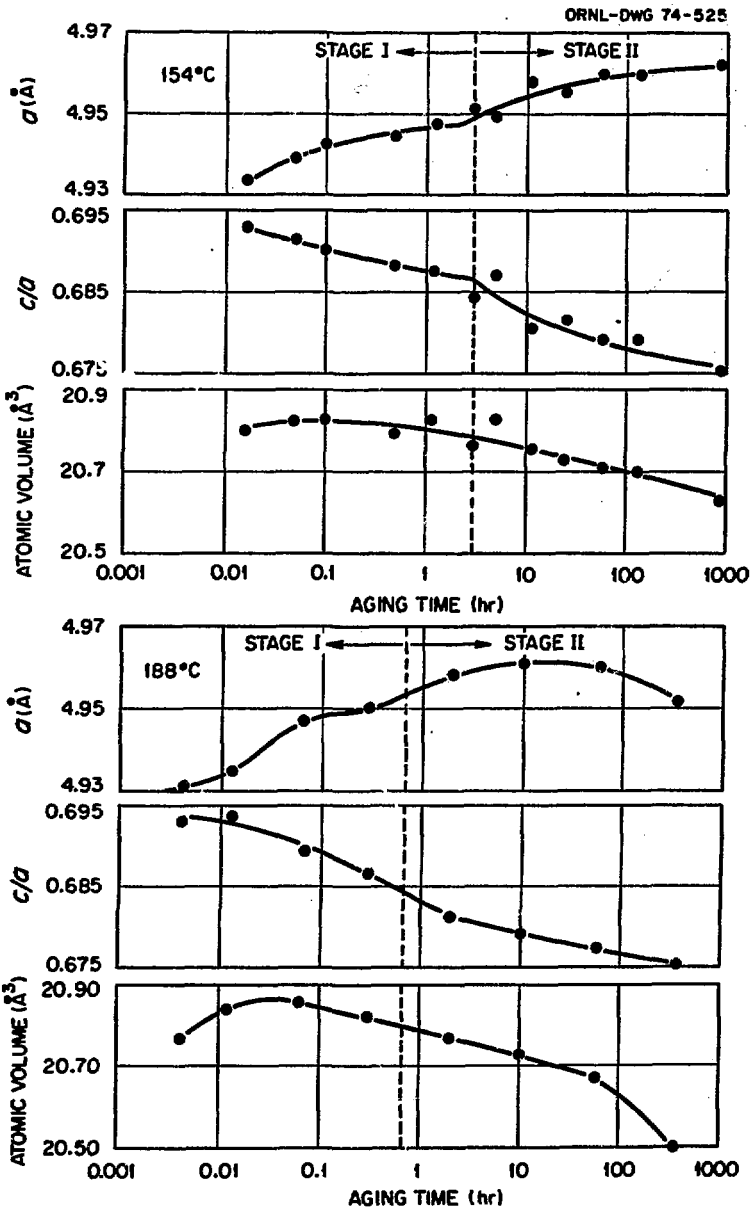
ORNL-DWG 74-525
154°C
STAGE I
STAGE II
a(Å)
4.97
4.95
4.93
c/a
0.695
0.685
0.675
ATOMIC VOLUME (Å³)
20.9
20.7
20.5
0.001
0.01
0.1
1
10
100
1000
AGING TIME (hr)
188°C
STAGE I
STAGE II
a(Å)
4.97
4.95
4.93
c/a
0.695
0.685
0.675
ATOMIC VOLUME (Å³)
20.90
20.70
20.50
0.001
0.01
0.1
1
10
100
1000
AGING TIME (hr)

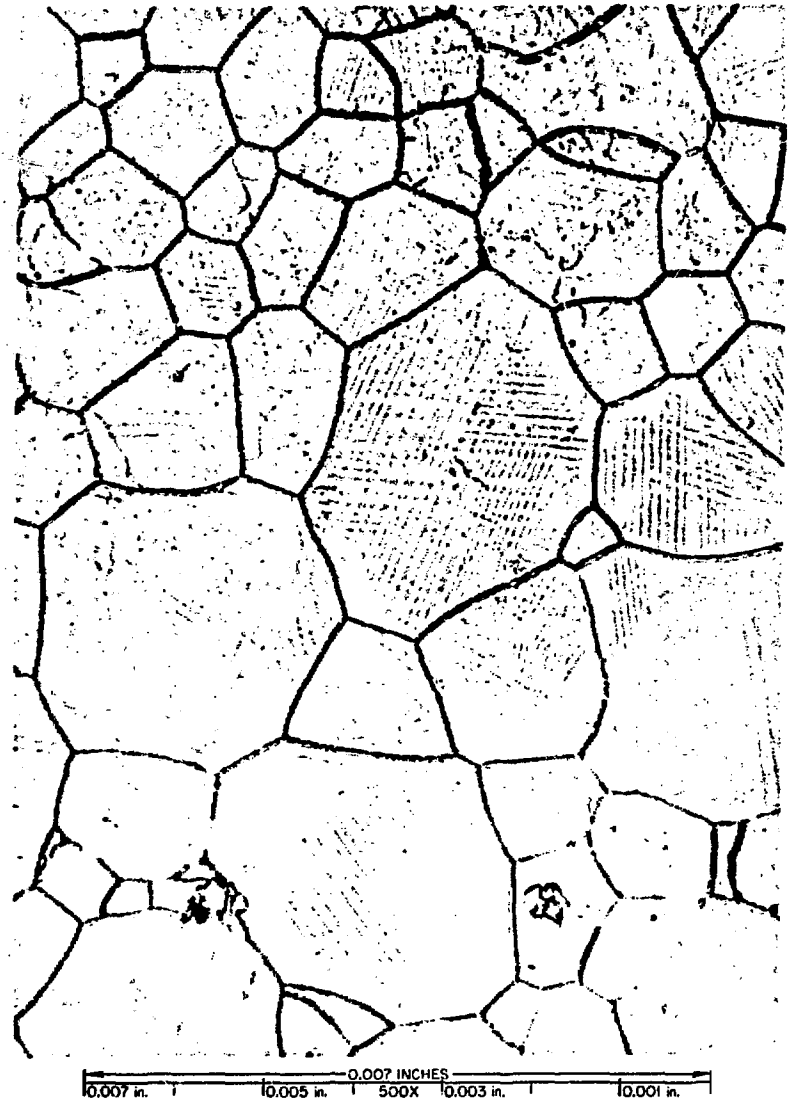
0.007 INCHES
0.007 in.
0.005 in.
500X
0.003 in.
0.001 in.

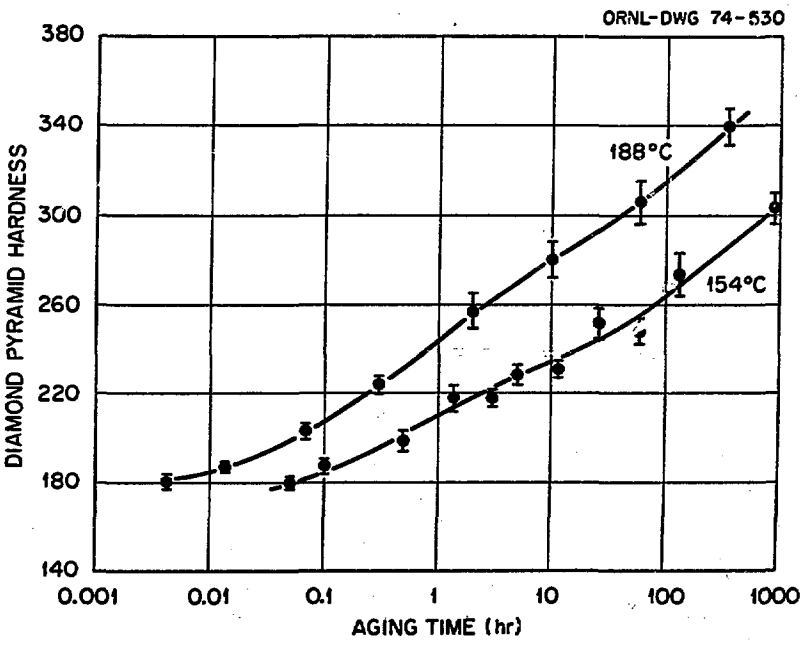
ORNL-DWG 74-530
380
340
300
260
220
180
140
DIAMOND PYRAMID HARDNESS
188°C
154°C
0.001
0.01
0.1
1
10
100
1000
AGING TIME (hr)

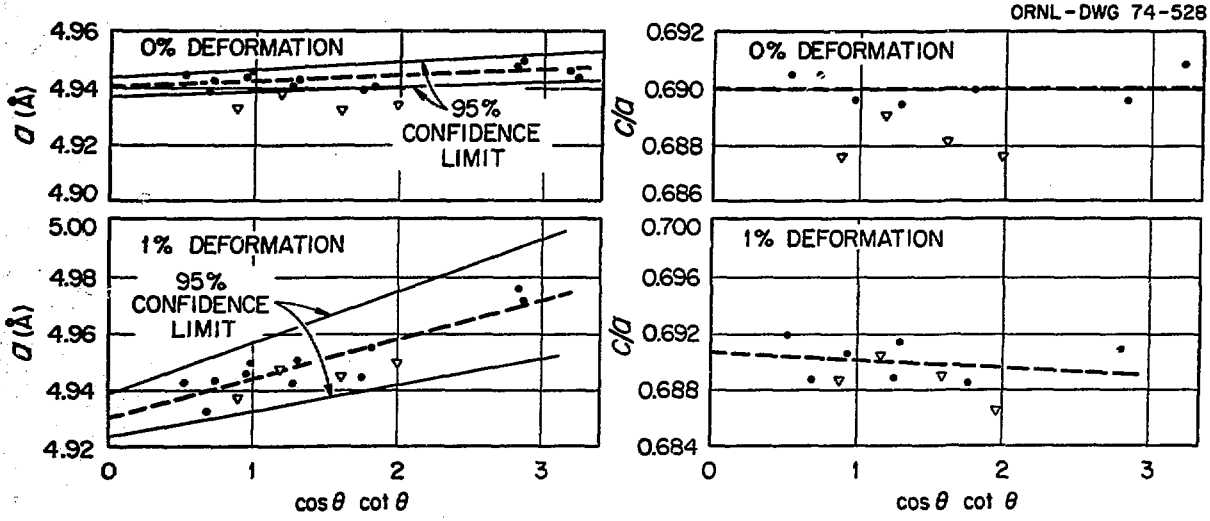
ORNL-DWG 74-528
0% DEFORMATION
95% CONFIDENCE LIMIT
1% DEFORMATION
95% CONFIDENCE LIMIT
a (Å)
c/a
cos θ cot θ
4.96
4.94
4.92
4.90
5.00
4.98
4.96
4.94
4.92
0.692
0.690
0.688
0.686
0.700
0.696
0.692
0.688
0.684
0
1
2
3

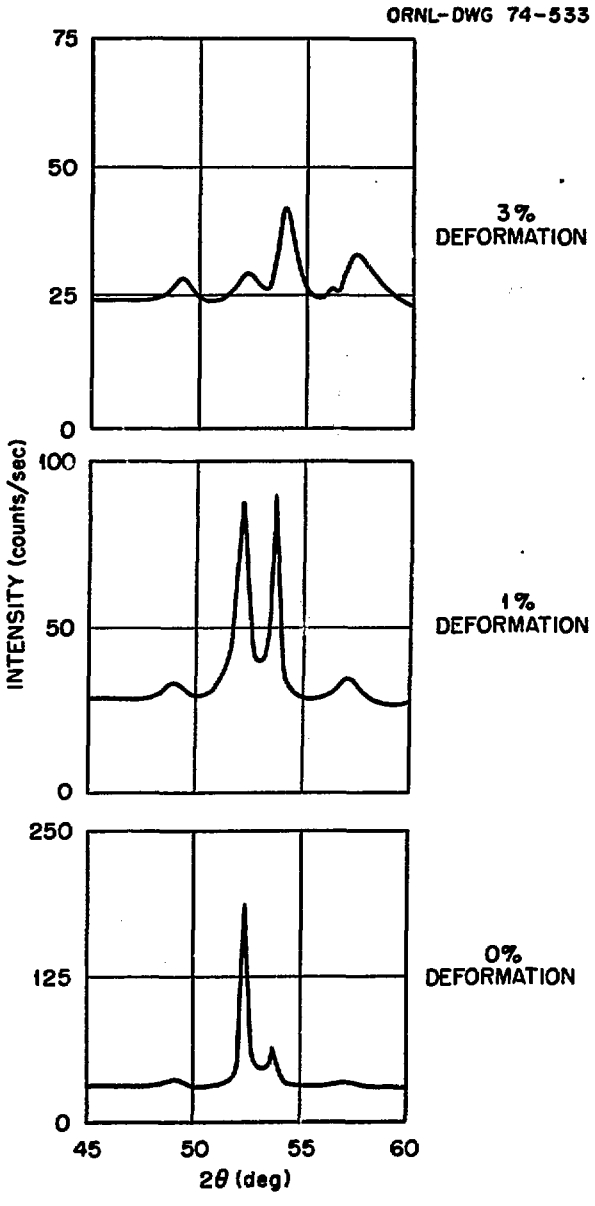
ORNL-DWG 74-533
75
50
25
0
3%
DEFORMATION
INTENSITY (counts/sec)
100
50
0
1%
DEFORMATION
250
125
0
0%
DEFORMATION
45
50
55
60
2θ (deg)

ORNL-DWG 74-534

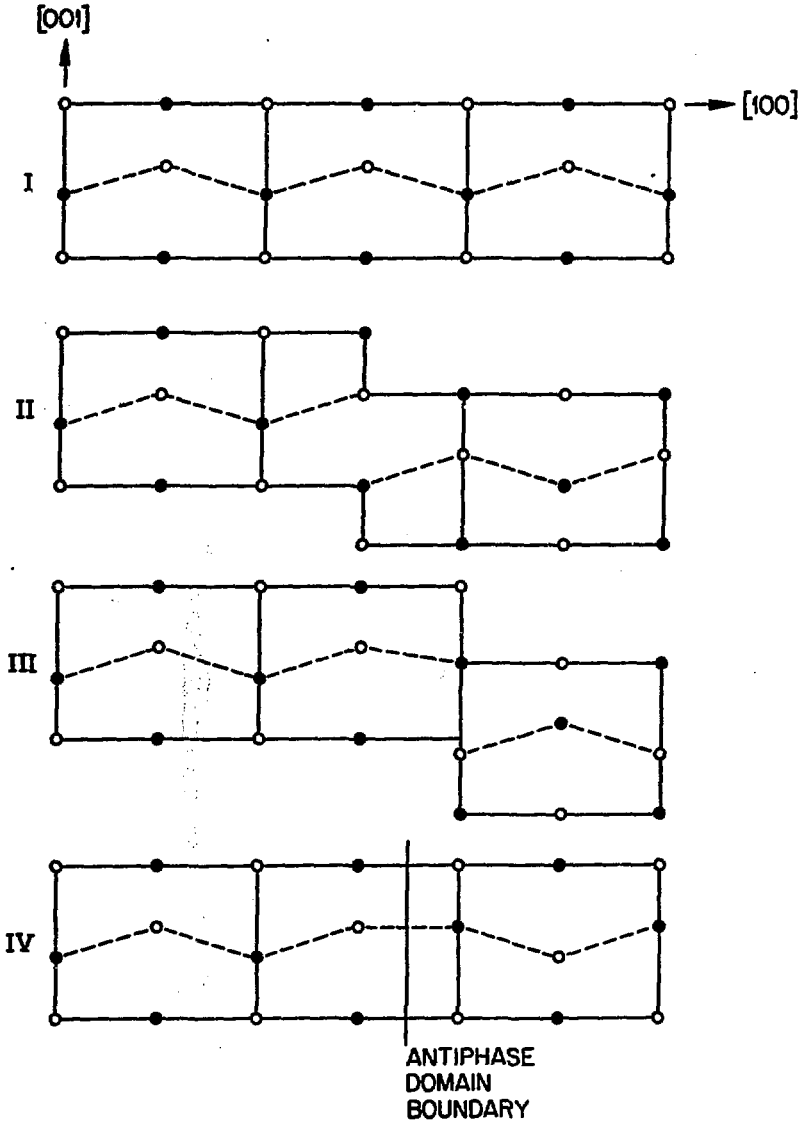

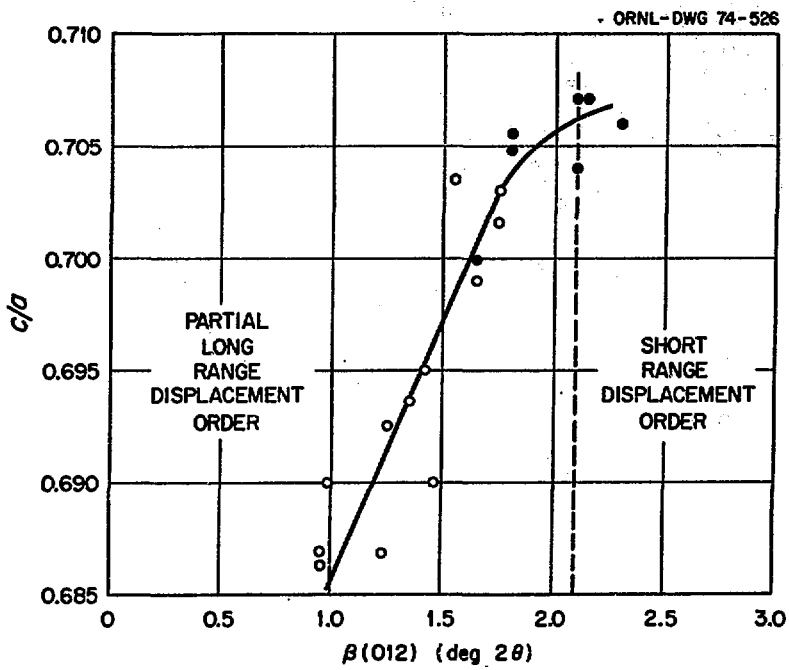
ORNL-DWG 74-526
0.710
0.705
0.700
0.695
0.690
0.685
c/a
PARTIAL
LONG
RANGE
DISPLACEMENT
ORDER
SHORT
RANGE
DISPLACEMENT
ORDER
0
0.5
1.0
1.5
2.0
2.5
3.0
β(012) (deg 2θ)

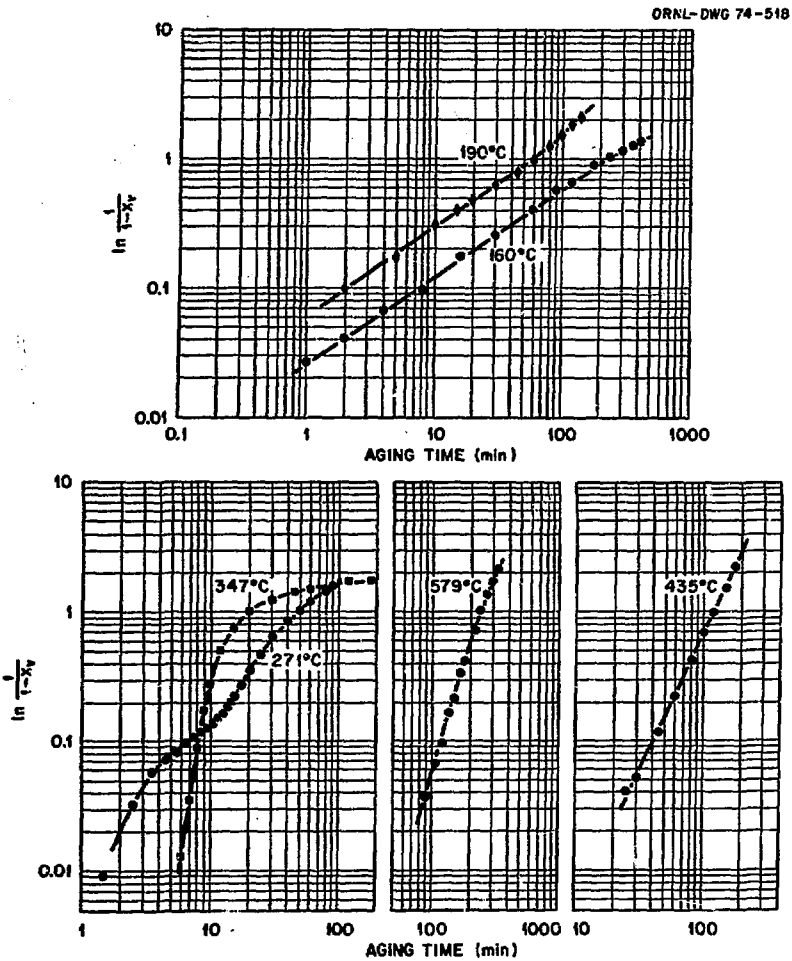
ORNL-DWG 74-518
10
1
0.1
0.01
$\ln \frac{f}{1-x}$
190°C
160°C
0.1
1
10
100
1000
AGING TIME (min)
347°C
271°C
579°C
435°C
1
10
100
1000

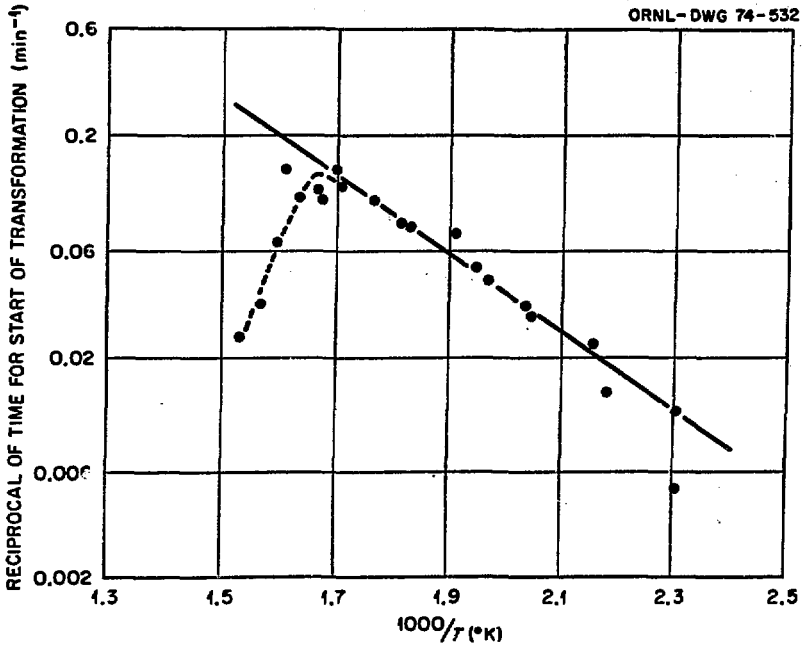
ORNL-DWG 74-532
RECIPROCAL OF TIME FOR START OF TRANSFORMATION (min⁻¹)
0.6
0.2
0.06
0.02
0.006
0.002
1.3
1.5
1.7
1.9
2.1
2.3
2.5
1000/T (°K)

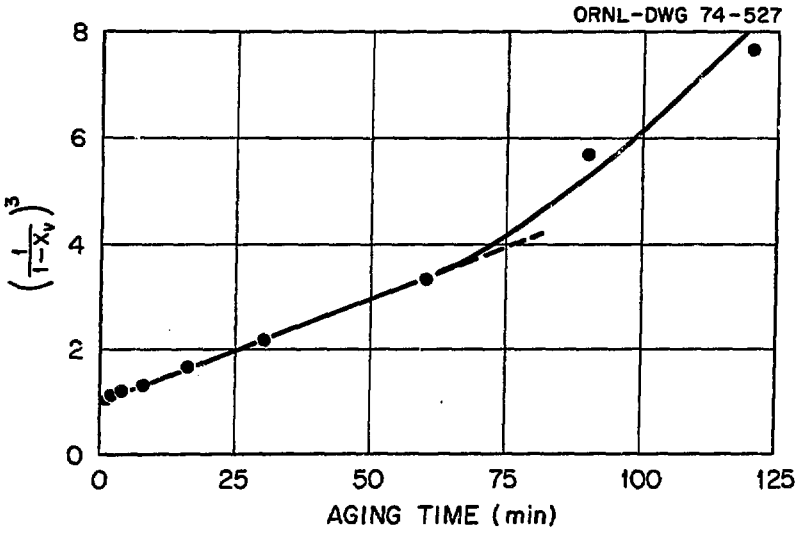
ORNL-DWG 74-527
8
6
4
2
0
0
25
50
75
100
125
AGING TIME (min)
$\left(\frac{1}{1-X_V}\right)^3$